

PATROLS 3202

Technical Description

DALI system: a description of the device and its characterisation

Table of Contents

1	SCOPE OF THE ANNEX	1
2	ABBREVIATIONS:	1
3	PRINCIPLE OF THE METHOD:	1
4	DESCRIPTION OF THE METHOD:	2
4.1	CHEMICALS AND REAGENTS USED:	2
4.2	APPARATUS AND EQUIPMENT USED:	2
4.3	PROCEDURE:	3
4.3.1	<i>An analytical model of the membrane displacement when applying a radial stretching</i>	3
4.3.2	<i>FEM Model of the bioreactor</i>	5
4.3.1	<i>Elements of the DALI System</i>	8
4.3.2	<i>Calibration of the membrane stretching system</i>	23
4.3.3	<i>QCM characterization and validation</i>	27
4.3.4	<i>Liquid and air tightness of the bioreactor</i>	31
5	REFERENCES	32

1 Scope of the Annex

This Annex presents the technical description of the DALI system, together with its characterization and validation from an engineering point of view.

2 Abbreviations:

BSA	Bovine Serum Albumin
DALI	Dynamic model for the ALveolar Interface
dH ₂ O	Distilled Water
FEM	Finite Element Method
FSI	Fluid Structure Interaction
NP	Nanoparticle
PBS	Phosphate-Buffered Saline
PC	Polycarbonate
PDMS	Polydimethylsiloxane
PLA	Polylactic acid
QCM	Quartz Crystal Microbalance
TD	Technical Description
UV	Ultraviolet

3 Principle of the Method:

A systematic characterization of the DALI system has been performed, validating the device from an engineering point of view. Before realizing the prototype, an analytical model of the membrane displacement related to the stretching was implemented. Moreover, a FEM model was developed to study the fluid dynamics in the bioreactor, considering also the changing in flow caused by the membrane displacement. The model was used to analyse the imbalance between air and hydrodynamic pressure, which causes the membrane to expand into the basolateral chamber. The analytical and computational models were used for supporting the system design and the understanding and prediction of the physical phenomena developing within the bioreactor.

Then, a prototype of the system was realized, and this annex aims at describing all its components and presenting the engineering characterization. A calibration of the

membrane stretching system was performed, and the liquid and air tightness of the bioreactor were verified. Finally, the designed QCM was characterized and validated, calculating its lower limit of the linearity range, its blank, and measuring nanoparticle deposition.

4 Description of the Method:

4.1 Chemicals and reagents used:

Liquid tightness of the Bioreactor:

- Phosphate-buffered saline (PBS)

QCM validation and characterization:

- Bovine serum albumin (BSA)
- Distilled water (dH₂O)
- Isotonic 0.9% NaCl solution
- Barium sulphate (BaSO₄) nanoparticles

4.2 Apparatus and equipment used:

DALI system (see Annex 3: SOP for assembly and use of DALI)

Calibration of the membrane stretching system:

- Infrared laser (GP2Y0A51SK0F, Sharp Electronics S.p.A., Milan, Italy)
- Manual linear micropositioner

Liquid tightness of the Bioreactor:

- Peristaltic pump (Ismatec IPC 4, IDEX Health & Science, Germany)
- Hydraulic circuit of the DALI system
- DALI control box

QCM validation and characterization:

- P1000, P200, P2.5 micropipettes
- 10 µL, 200 µL and 1000 µL pipette tips
- Hot plate
- QCM200 controller
- Nebulizer (Aeroneb Pro, Aerogen, Galway, UK) and its controller (Aerogen® Pro-X, Aerogen, Galway, UK)

4.3 Procedure:

4.3.1 An analytical model of the membrane displacement when applying a radial stretching

In order to predict the stimuli applied to the cell layer, membrane displacement can be correlated to the radial stretching of the membrane. Considering a sphere of radius r , the deformed membrane can be assumed as the surface area of a spherical section of the sphere (Figure 1). This assumption is valid until the chord length of the spherical section (h in Figure 1, corresponding to the maximal displacement of the membrane) is shorter than the membrane radius (a in Figure 1):

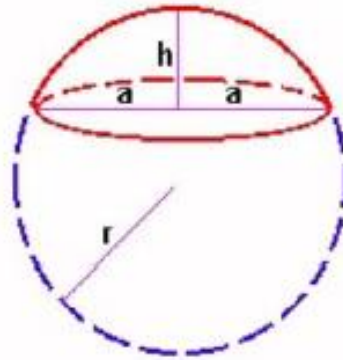


Figure 1: Spherical cap sketch.

Starting from this assumption, the deformed area of the membrane (S_{lat}) can be viewed as a function of the initial area (A) and its increment (δA) (Eq. 1 and 2).

$$S_{lat} = \pi \cdot (a^2 + h^2) \quad (1)$$

$$S_{lat} = A + \delta A = \pi a^2 + \delta A \quad \rightarrow \quad \delta A = \pi h^2 \quad (2)$$

The *surface strain* ($\varepsilon_{\Delta S}$, distension area) is given by the ratio between the area and its increment (Eq. 3), allowing to write the maximal membrane displacement h as a function of the membrane radius and the *surface strain* (Eq. 4).

$$\varepsilon_{\Delta S} = \frac{\delta A}{A} \quad \rightarrow \quad \delta A = \varepsilon_{\Delta S} \cdot A = \varepsilon_{\Delta S} \cdot \pi a^2 \quad (3)$$

$$\pi h^2 = \varepsilon_{\Delta S} \cdot \pi a^2 \quad \rightarrow \quad h = a \sqrt{\varepsilon_{\Delta S}} \quad (4)$$

In mechanics, assuming an isotropic expansion, the linear strain ε is expressed as in Equation 5 [1], allowing to obtain the maximal displacement in terms of linear strain $(\delta r/r)$ (Eq. 6):

$$\varepsilon = \sqrt{1 + \varepsilon_{\Delta S}} - 1 \quad (5)$$

$$\varepsilon_{\Delta S} = (\varepsilon + 1)^2 - 1 = \varepsilon^2 + 2\varepsilon = \left(\frac{\delta r}{r}\right)^2 + 2\frac{\delta r}{r} \rightarrow h = a\sqrt{2\frac{\delta r}{r} + \left(\frac{\delta r}{r}\right)^2} \quad (6)$$

Since $\left(\frac{\delta r}{r}\right)^2$ tends to zero, it can be neglected; for this reason, Equation 7 becomes:

$$h = a\sqrt{2\frac{\delta r}{r}} \quad (7)$$

Equation 7 allows to correlate the maximal membrane displacement h with the linear strain of its surface. Moreover, the maximal axial deformation permits the quantification of the volume occupied by the membrane in the basolateral chamber during breathing.

Studies of alveolar epithelial cell cultures exposed to mechanical strain *in vitro* suggest that a 25% increase in cell surface area corresponding to 8-12% linear distension likely correlates with physiological levels of mechanical strain experienced by alveolar epithelium [2]. In general, physiological levels of strain can be assumed between 5 and 12% [3]. Under this level, cells will be understretched, while increasing the linear distention (>17%) lead to pathophysiological conditions [2], [3]. Equation 7 allows to obtain the axial displacement of the membrane considering these reference linear strains (5, 12 and 17%). In order to compare the results obtained with the DALI system to the standard static cultures in transwells, the device is based on the dimensions of a six-well Transwell insert. Therefore, the membrane radius was set equal to 12 mm. Considering the radius $a = 12$ mm, we obtain:

- Linear strain: 5% \leftrightarrow 0.05 $\rightarrow h = 12 \cdot \sqrt{2 \cdot 0.05} = 3.79$ mm
- Linear strain: 12% \leftrightarrow 0.12 $\rightarrow h = 12 \cdot \sqrt{2 \cdot 0.12} = 5.88$ mm
- Linear strain: 17% \leftrightarrow 0.17 $\rightarrow h = 12 \cdot \sqrt{2 \cdot 0.17} = 7$ mm

To conclude, the maximum membrane displacement in the z-direction that needs to be reached to replicate pathological conditions is 7 mm. Therefore, bioreactor

basolateral chamber must be dimensioned considering this encumbrance during membrane expansion. The geometry of the bioreactor prototype reported in the following section was designed considering this aspect.

4.3.2 FEM Model of the bioreactor

4.3.2.1 Methods

A FEM model was used to simulate membrane displacement due to the pressure imbalance on the two sides of the air/liquid interface. The model of the bioreactor is based on the fluid structure interaction (FSI) module of COMSOL Multiphysics 5.3 software. The model is represented by a cylindrical chamber, with a diameter of 24 mm and a height of 20 mm (see section 4.3.1.1). The compartment is connected to the external system with an inlet and an outlet (5 mm in diameter). The membrane is modelled as a disk on the top of the bioreactor and undergoes a constant pressure from the top (simulating the constant pressure into the apical chamber). The fluid flows from the inlet to the outlet tube, perfusing the chamber, and imposes a force on the membrane wall resulting from the viscous drag and fluid pressure. However, the deformable membrane bends under the applied load. Consequently, the pressure gradient is different from the free-standing material, generating a different membrane displacement, and fluid flow also follows a new path. The inlet velocity is fixed at 400 $\mu\text{L}/\text{min}$ [4], and the fluid dynamics is solved in the Laminar Flow regime, due to the small velocity in the chamber (Reynolds number < 1). Bioreactor walls are set as walls with the no slip condition and water was chosen as a reference fluid. The fluid dynamic constants and the membrane characteristics are shown in Table 1. In particular, the Young's modulus and the thickness of the membrane were derived from its characterisation presented in Annex 4 (TD): *Preparation and mechanical characterization of Bionate membranes*.

Table 1: Fluid dynamic constants and membrane characteristics.

Fluid viscosity	$10^{-3} \text{ Pa}\cdot\text{s}$
Fluid density	$1000 \text{ Kg}/\text{m}^3$
Temperature	$37 \text{ }^\circ\text{C}$
Membrane Thickness	$75 \text{ }\mu\text{m}$
Membrane Young's Modulus	1.4 MPa
Membrane Poisson's Ratio	0.495

The FEM model was solved for different pressures (1 to 15 kPa with a step of 1 kPa), in order to establish the pressure at which the membrane displacement in z-direction is 7 mm. As mentioned in section 4.3.1, this value corresponds to a linear distention of $\approx 17\%$, mimicking pathological levels of stretching [2], therefore the maximum that needs to be reached. In correspondence of the membrane domain, the mesh was set as *Extra fine* (minimum element size: $6.3 \cdot 10^{-2}$ mm, maximum element size: 1.47 mm), scaling the geometry of the finite elements in the z-direction of a factor 3, since the thickness of the membrane is equal to $7.5 \cdot 10^{-2}$ mm. In the remaining domains, the mesh was set as *Normal* (minimum element size: 0.76 mm, maximum element size: 4.2 mm). The number of finite elements of the final mesh are summarized in Table 2.

Table 2: Number of elements of the final mesh.

Number of domain elements	182876
Number of boundary elements	40058
Number of edge elements	740

4.3.2.2 Results

Figure 2 shows the total membrane displacement at 10.6 kPa, which corresponds to the z-displacement of 7 mm. When the pressure in the apical chamber increases, the membrane stretches, moving into the basolateral chamber, until it reaches an equilibrium with the hydrodynamic pressure of the flowing liquid.

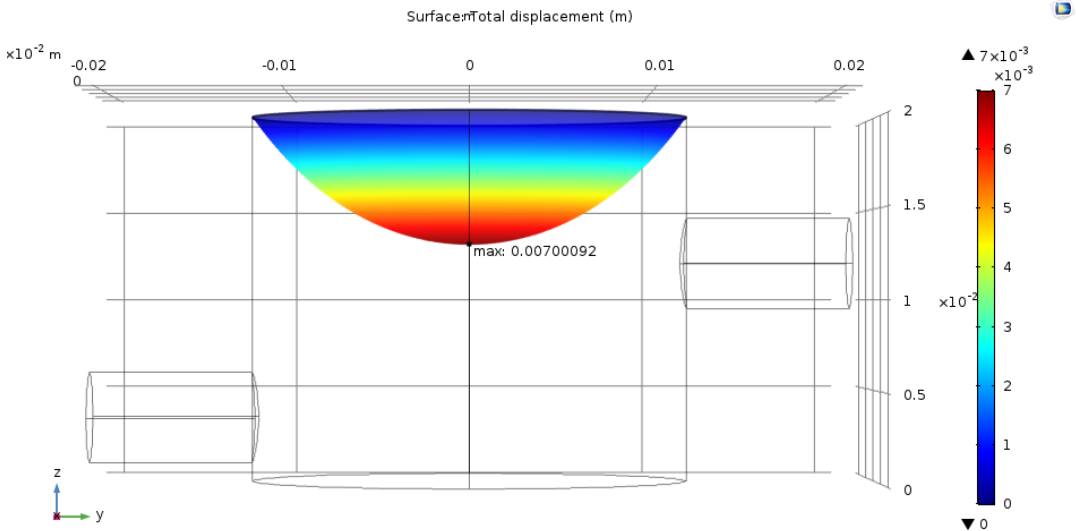


Figure 2: Total displacement of the membrane.

The model was then used to evaluate the shear stresses over the bottom side of the membrane (endothelial side), which is the one in contact with the flowing media. When the membrane is not pressurized, the model predicts a maximum shear stress of $1.35 \cdot 10^{-4}$ Pa in the central region of the membrane. When the membrane is stretched with a linear strain of 17%, the shear stress in the central region is $1.19 \cdot 10^{-4}$ Pa. Computed shear stress values result lower than the typical physiological shear stresses reported in the literature for endothelial cells (~ 1.5 Pa) [5]. However, even values lower than $2 \cdot 10^{-4}$ Pa [6] have been reported to have significant positive effects on the growing cells with respect to static controls. Figure 3 shows the color maps of the shear stress distributions in case of relaxed and stretched membrane.

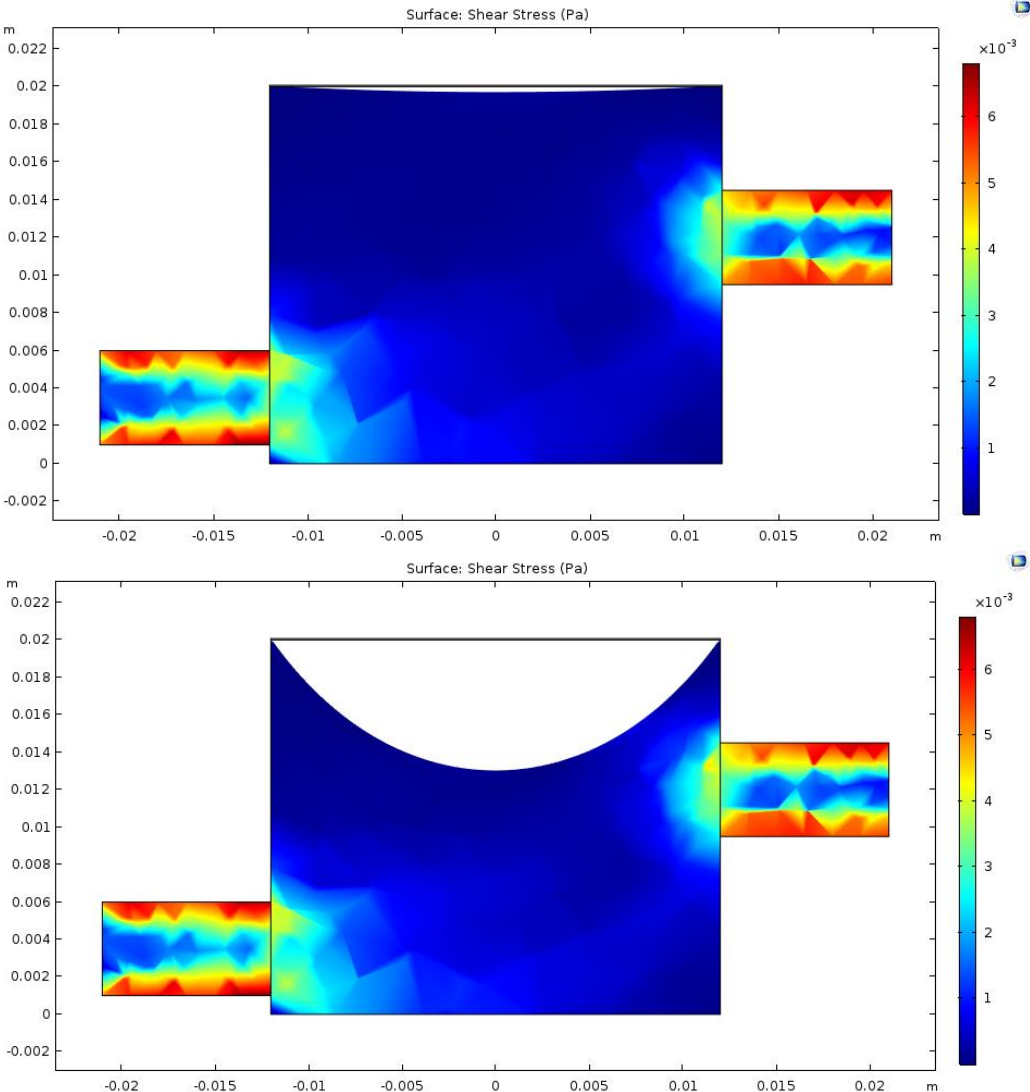


Figure 3: Color maps of the shear stress distributions in case of relaxed (on top) and stretched membrane (on bottom).

Finally, Figure 4 shows the velocity field of the fluid flowing through the basolateral chamber, considering both the non-stretched and stretched (linear strain of 17%) membrane condition. Regions in which the density of streamlines is high are characterized by high fluid velocity and hence greater convective transport.

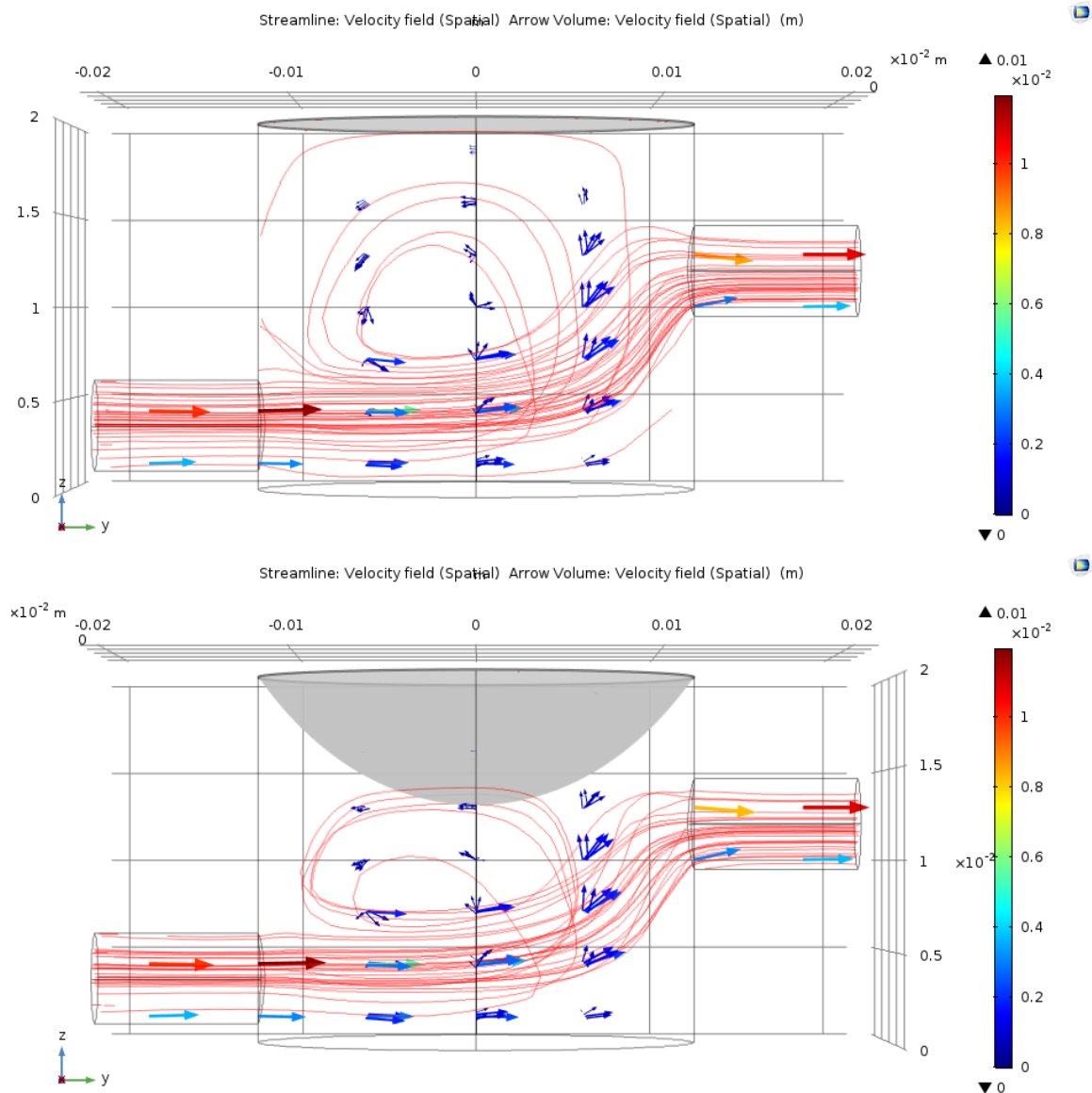


Figure 4: Velocity field in the basolateral chamber: non-stretched membrane on top, stretched membrane on bottom.

4.3.1 Elements of the DALI System

In the following sections all the elements of the designed system are presented in detail (Figure 5): the bioreactor chambers, membrane holder, hydraulic circuit, aerosol nebulizer, QCM and control box.

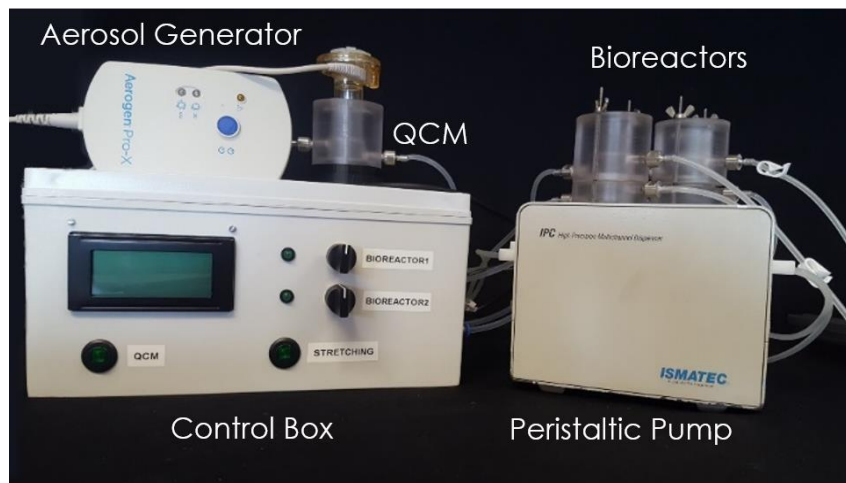


Figure 5: Picture of the DALI system, showing all its elements: the bioreactors, peristaltic pump, QCM, aerosol generator and control box.

4.3.1.1 Bioreactor chambers, hydraulic circuit and membrane holder

SolidWorks 2017 software (Dassault System, Vlizy-Villacoublay, France) was used to design the bioreactor prototype. The cylindrical chambers were dimensioned like a 6-well Transwell insert (diameter = 24 mm) to facilitate biologists who generally use these formats. The apical chamber was designed to directly connect a commercial nebulizer. A collector was integrated to the upper chamber to connect the bioreactor to the nebulizer. The height of the apical chamber, together with the one of the collector, were optimized in order to have a homogeneous distribution of the aerosolised nanoparticles. On the other side, the basolateral chamber was dimensioned considering membrane encumbrance during its displacement. Both apical and basolateral chambers have an inlet and an outlet. Considering the fluidic side, the inlet and outlet allow media flow through the basolateral chamber, from the first to the second; if considering the apical side, the inlet allows air inflow into the apical chamber leading to membrane stretching, while the outlet is generally closed. This avoid air outflow during the pressurisation of the apical chamber. The apical chamber of the bioreactor was designed with an outlet in case the system would use in other applications in which a dual flow is needed (e.g. intestine *in vitro* model). Figure 6 shows a schematic view of the bioreactor prototype with the fundamental dimensions and its SolidWorks sketch.

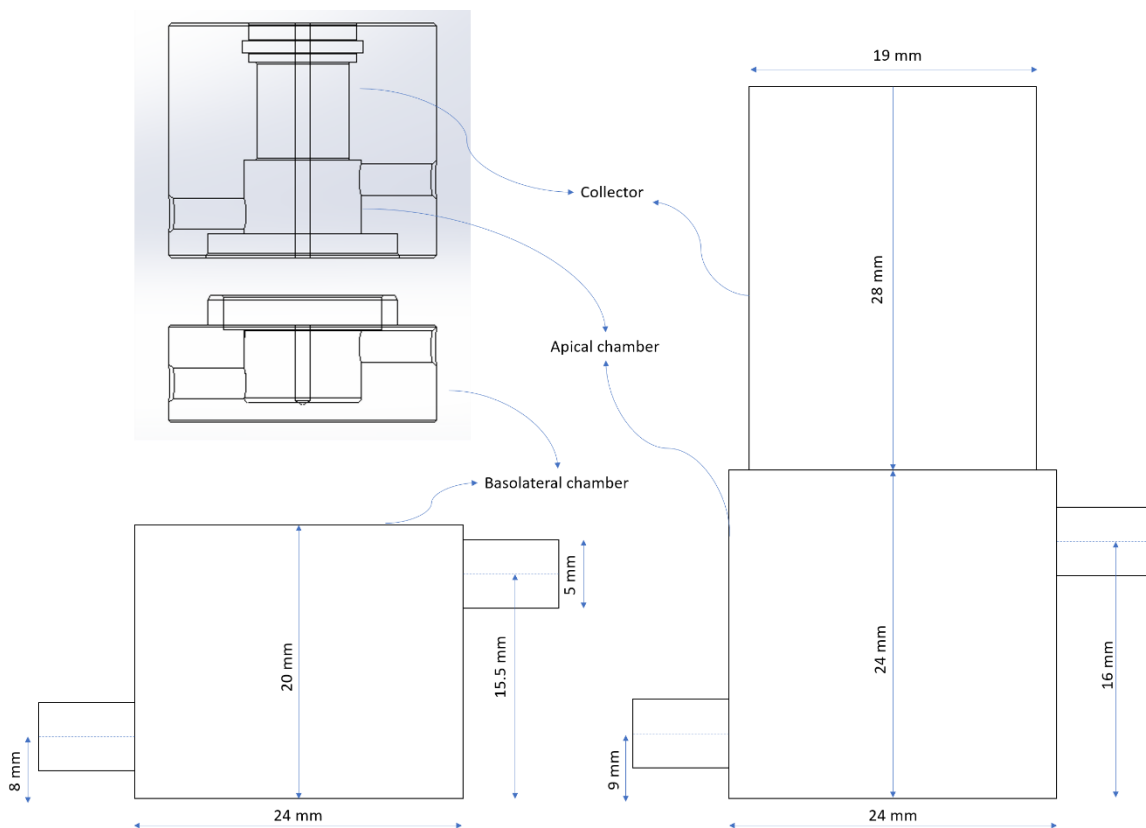


Figure 6: Schematic view and SolidWorks sketch of the basolateral and apical chambers of the bioreactor. The fundamental dimensions are summarized in the schematic view.

The bioreactor chambers were fabricated from a PC bar by subtractive manufacturing (machine tools). The bioreactor chambers are cylindrical with rounded edges, in order to facilitate cleaning procedures after their use.

The apical chamber (Figure 7) is connected to an electropneumatic regulator (ITV0011-2BL, SMC, Italy), allowing a pressure-controlled airflow for membrane stretching. The collector (Figure 7a) integrated to the upper chamber connects the bioreactor to the nebulizer. When the nebulizer is not connected to the bioreactor, the collector is closed by a cap obtained by PDMS (Sylgard 184 kit, Mascherpa, Milano, Italy) moulding. The basolateral chamber (Figure 7) simulates the blood side of the alveolar barrier, therefore it is connected to a hydraulic circuit allowing for continuous flow of cell culture medium using a peristaltic pump (Ismatec IPC 4, IDEX Health & Science, Germany).

The inlets and outlets of the chambers are made of stainless steel, in order to avoid oxidation in a humid environment, and were obtained by subtractive manufacturing

(Figure 7a). The inlets and outlets are connected to silicone tubes and the outlet of the apical chamber is generally closed by a clip as shown in Figure 7a.

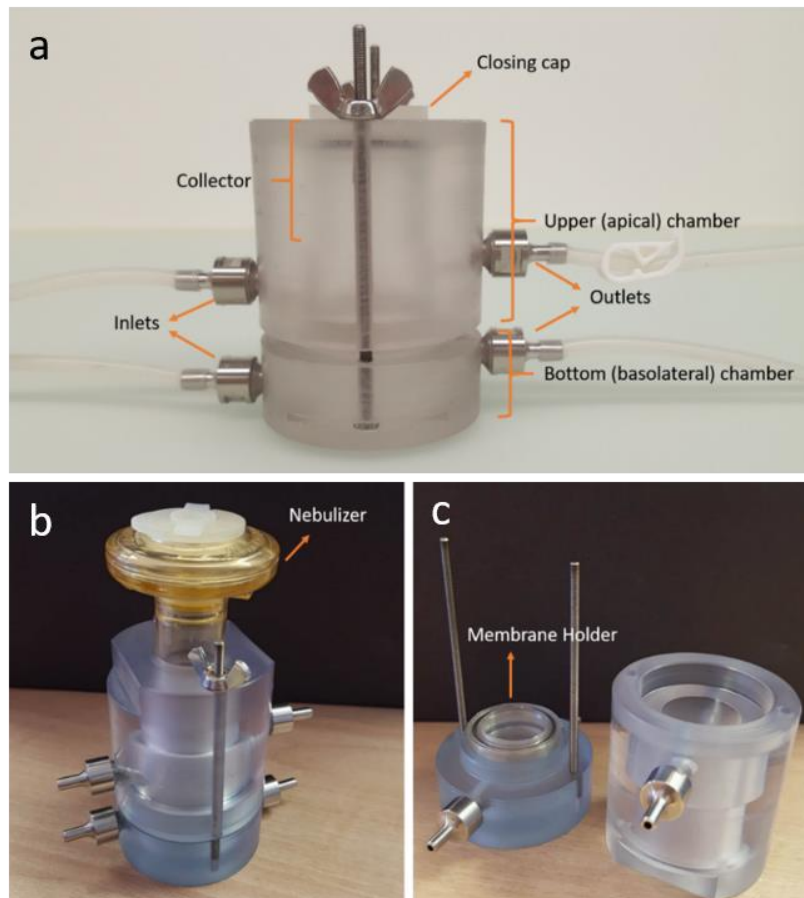


Figure7: Pictures of the designed bioreactor: (a) closed bioreactor where its elements are shown, (b) closed bioreactor connected to the nebulizer, (c) opened bioreactor showing the membrane holder.

Besides the pump, the hydraulic circuit is composed of silicone tubes (the hydraulic tubes, inner diameter: 2 mm, outer diameter: 4 mm) and a medium reservoir (Figure 8), which is used as a liquid reserve and oxygen exchange point. The reservoir is a modified commercial bottle (Nalgene™, Thermo Fisher Scientific, Waltham, MA, USA) which was provided with 3 silicone tubes: an inlet tube (inner diameter: 2 mm, outer diameter: 4 mm), an outlet tube (inner diameter: 1 mm, outer diameter: 3 mm) and a filter tube (inner diameter: 2 mm, outer diameter: 4 mm), as shown in Figure 8. These tubes are sealed to the bottle thanks to a layer of polymerized PDMS. The inlet and outlet tubes allow medium inflow and outflow and have different dimensions to easily distinguish them during the assembly of the system. A syringe filter is placed on the filter tube to allow medium oxygenation avoiding any contamination. The

reservoir has a capacity of 60 mL, a closure size of 28 mm and is made of polypropylene (PPCO).

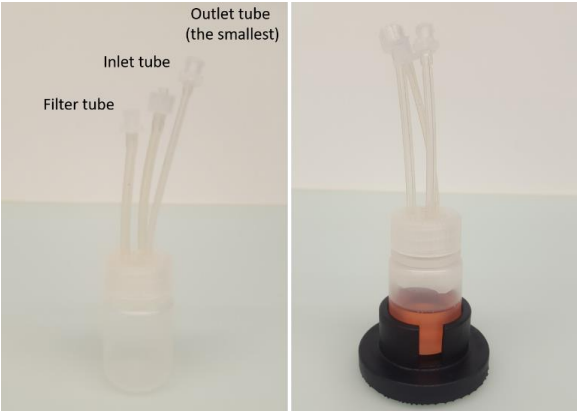


Figure 8: Picture of the reservoir and its 3 tubes: the inlet tube, the outlet tube and the filter tube. On the right: the reservoir filled with medium and held in a 3D printed case.

Using the previously mentioned hydraulic tubes, the outlet tube of the reservoir is connected to the inlet tube of the basolateral chamber (on top in Figure 9), while the inlet tube of the reservoir to the outlet tube of the bioreactor, placing the pump in between (Figure 9, below). Therefore, the medium flows from the outlet tube of the reservoir to the inlet of the bioreactor, through the basolateral chamber and again to the reservoir, thanks to the peristaltic pump.

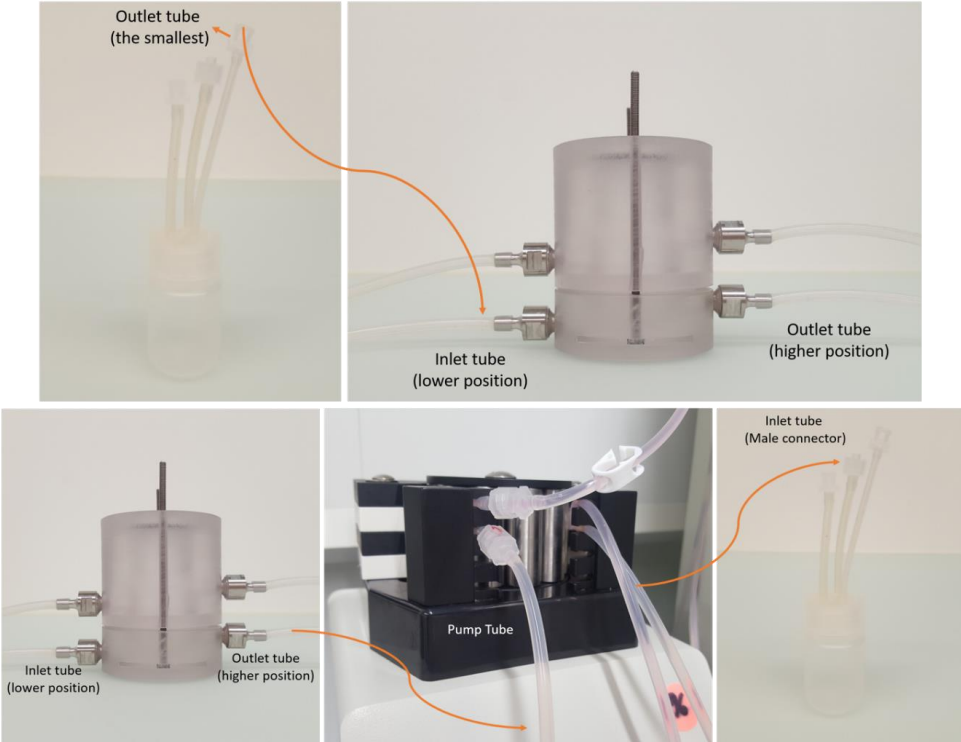


Figure 9: Connection of the bioreactor to the hydraulic circuit.

Cross contamination has been avoided fabricating more than one device to be used in parallel during experiments. With a single control unit, it is possible to control 2 bioreactors in parallel. In this way, different samples have their own cell culture media and air source, avoiding cross contamination.

Considering the membrane holder, it consists of two annular neodymium magnets (ITALIFIT magneti srl, Fagnagna, Italy) covered by PDMS (Dint: 24 mm, Dext: 32 mm, Figure 10). To obtain the holder, PDMS was poured into a mould for 1/3 of its height and let polymerize. Then, the magnet was placed on the cross-linked PDMS and completely covered with other PDMS, until the filling of the mould. After the polymerization, the magnet covered by PDMS was removed from the mould. When the membrane is fixed in the holder, it can be easily handled without being damaged. It can be placed in a 6-well Transwell to perform static experiments, or between the two chambers of the bioreactor during dynamic culture.



Figure 10: Picture of the selected membrane holder.

The bioreactor is closed by tightening wing nuts, and its tightness is ensured by the presence of the membrane holder enclosed in PDMS, which is self-adhesive and deformable.

The moulds used to obtain the closing cap and the holders were designed with SolidWorks and printed with the Ultimaker 3D printer. The silicone poured into the moulds was prepared according to the manufacturer's instructions (1:10 PDMS monomer-catalyzer mix).

All the components can be sterilized by autoclaving, gas plasma, UV light or with a 70% ethanol solution. The only exception refers to the holder, which cannot be autoclaved since neodymium magnets degauss at temperature higher than 80°C.

4.3.1.2 Aerosol system

In order to study the effects of aerosols on lung cells, a commercial system was used able to aerosolize both drugs and NPs on the cell layer. The selected commercial aerosol system is composed of a nebulizer (Aeroneb Pro, Aerogen, Galway, UK) and a controller (Aerogen® Pro-X, Aerogen, Galway, UK) (Figure 11). The nebulizer is connected both to the bioreactor (Figure 7b), ensuring tightness thanks to a plastic O-ring, and to the controller. With the Aerogen® Pro-X, it is possible to select an aerosolization of 30 minutes or use the continuous mode. The nebulizer holds up to 10 mL of liquid, it is translucent to allow visual monitoring of substance levels, and it can be sterilized by autoclaving. When the nebuliser is connected into the breathing circuit, the filler cap can be opened or removed from the nebuliser without causing loss of circuit pressure.

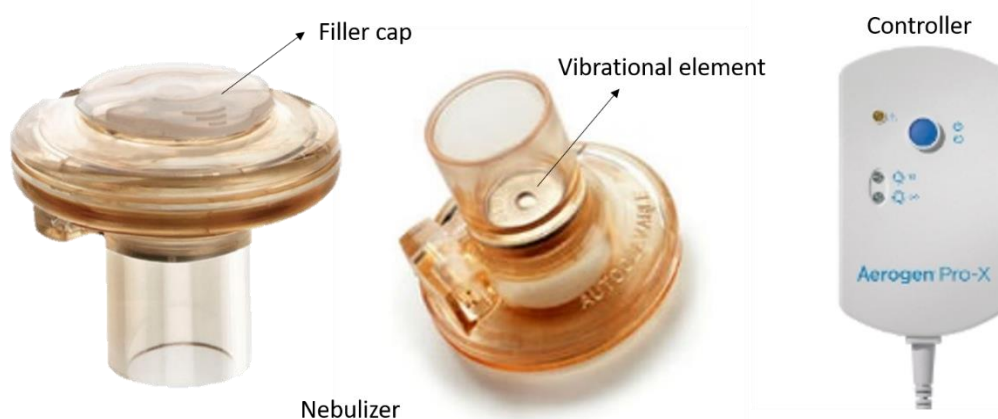


Figure 11: The nebulizer and the controller are the two elements of the aerosol system.

4.3.1.3 Quartz Crystal Microbalance

The dosing of NPs is crucial for understanding their effects on the cells, and for correlating a specific dose of NPs to a pathological or physiological state. Therefore, in order to quantify the amount of aerosolised particles on the cell layer, a Quartz Crystal Microbalance was integrated to the system, since it is able to detect amounts in the order of nanograms. In particular, the QCM comprises a thin piezoelectric quartz crystal (Figure 12) in contact with two metal electrodes that establish an alternating electric field across the crystal, causing vibration at its resonant frequency [2]. This resonant frequency is sensitive to mass changes at nanogram level and, therefore, QCM is used to measure deposition rates.

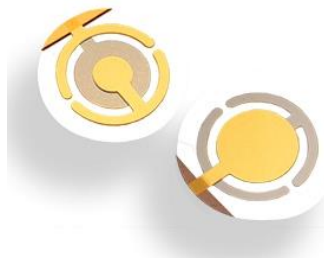


Figure 12: Picture of a piezoelectric quartz crystal.

The QCM (Figures 13 and 14) is composed by:

- A piezoelectric quartz crystal (Figures 13 and 14), whose characteristics are summarized in Table 3. The selected crystal has a diameter equal to 25.4 mm: in this way it was possible to compare the amount of aerosolized particles on the crystal and on the membrane, since they have a similar deposition area (the diameter of the membrane where cells are seeded is 24 mm). It was not possible to have the same deposition area since the commercial crystals have standard dimensions.

Table 3: Quartz Crystal characteristics.

Fundamental frequency	5 MHz
Crystal diameter	25.4 mm
Crystal thickness	333 μ m
Front Electrode Diameter	12.7 mm
Overtone order in the TSM (<i>n</i>)	1

- Two spring electrodes in contact with the crystal (Figure 13).
- A support made of PLA where the electrodes and the crystal are placed (black component in Figure 13 and 14). It was 3D printed with the Ultimaker 3D printer and connected to a commercial digital controller.
- The upper chamber of the bioreactor fixed to the support element and connected to the nebulizer (Figure 13). The presence of O' rings guarantees the tightness between the support and the chamber (Figure 13). As previously explained, I decided to use the upper chamber as connection to the nebulizer, in order to have a comparable distribution of NPs on the crystal and on the cells seeded on the membrane.
- A commercial digital controller (QCM200, Stanford Research Systems, SRS, Sunnyvale, CA) with a built-in frequency counter and resistance meter. The

QCM200 can be operated from the front panel or a PC using the RS-232 interface. The controller is provided with a Windows software for real-time data acquisition, display, analysis and storage. Both frequency and resistance trends can be viewed.

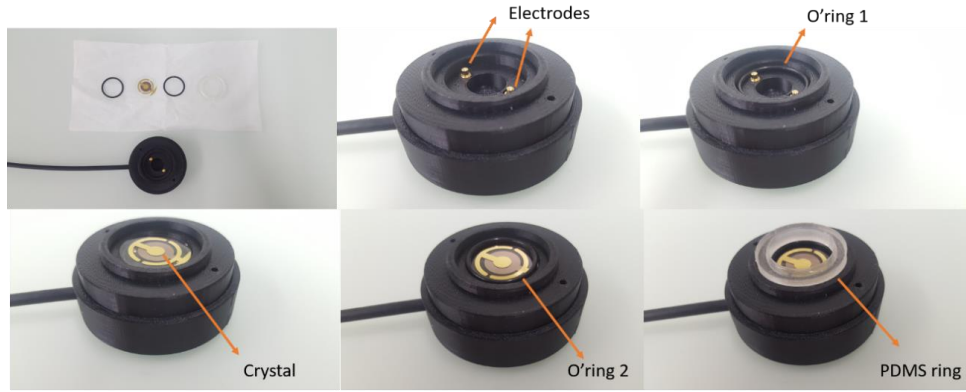


Figure13: Assembling of the designed QCM.

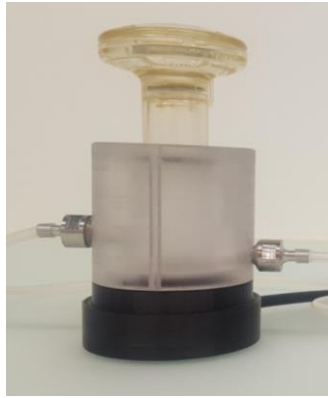


Figure14: Assembled QCM.

Using the Sauerbrey equation (Eq. 8) and the quartz crystal characteristics summarized in Table 3, it is possible to derive the mass change (Δm) on the surface of the electrode as follow (Eq. 9):

$$\Delta f = -\frac{2f_0^2}{A\sqrt{\rho\mu}} \cdot n \cdot \Delta m = -2.26 \cdot 10^{-6} \cdot n \cdot f_0^2 \cdot \frac{\Delta m}{A} \quad (8)$$

$$\Delta m = \frac{\Delta f \cdot A}{-2.26 \cdot 10^{-6} \cdot n \cdot f_0^2} = \frac{\Delta f \cdot \left(\frac{12.7}{2}\right)^2 \pi}{-2.26 \cdot 10^{-6} \cdot 1 \cdot 5^2} \quad (9)$$

Where Δf is the frequency shift measured with the designed QCM.

Figure 15 shows the commercial controller connected to its crystal holder (in the orange box), which was replaced by the described QCM. Using the designed device instead of the commercial crystal holder it was possible to have a realistic prediction of the amount of the aerosolized particles on the membrane, as the membrane and the crystal are at the same position, and the QCM has the same geometry of the bioreactor (Figure 16).



Figure 15: The commercial controller of the QCM. In the box is shown the crystal holder replaced by the designed device.

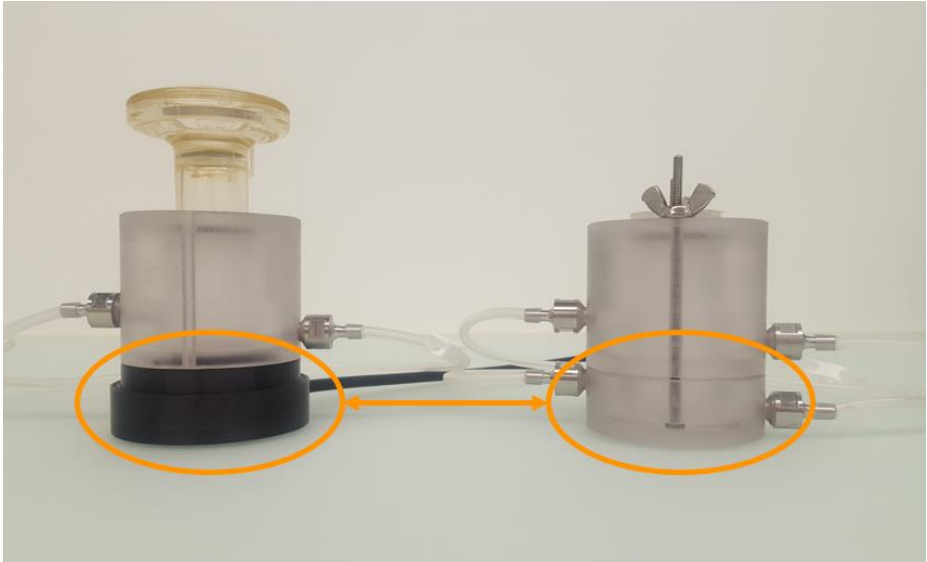


Figure 16: On the left is shown the QCM, while on the right the bioreactor. It is possible to appreciate the similar geometry of the devices, designed to have predictable measurements of the amount of aerosolized nanoparticles.

It is also possible to directly connect the QCM to the control box (see section 4.3.1.4 - QCM parameters acquisition), having the possibility to read the frequency directly on its LCD without using the commercial controller. However, using the commercial

controller it is also possible to evaluate the entire trend as showed by its software (Figure 17).

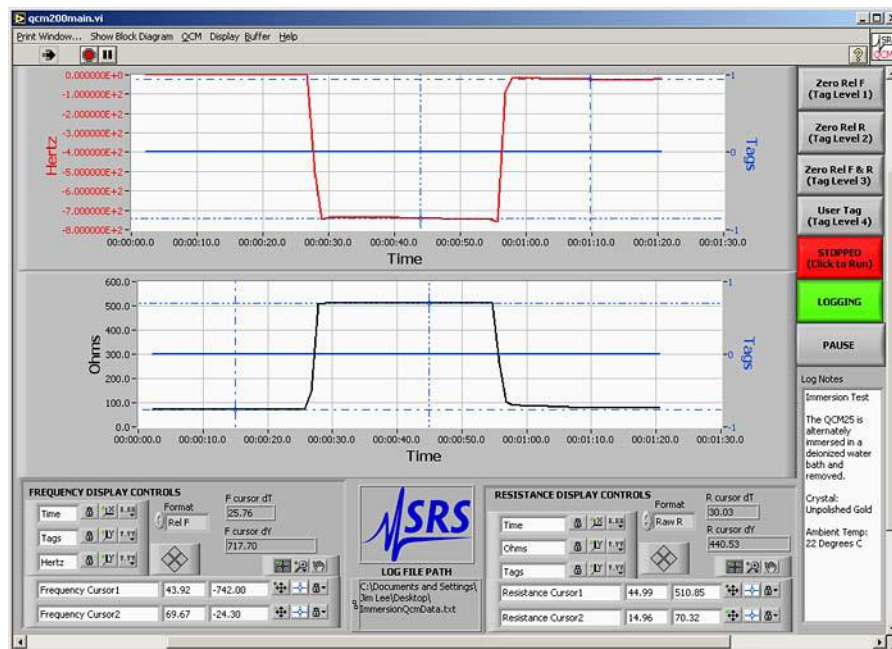


Figure 17: Software panel showing the frequency (top) and resistance (bottom) trends.

Finally, since the resonant frequency of the crystal depends on the external temperature, the control unit contains a temperature sensor that allow to monitor this parameter (more details in section 4.3.1.4 – QCM parameter acquisition)

4.3.1.4 Control Box

A control unit is necessary to allow the communication between the operator and the actuation system for the culture environment. Therefore, a control box was designed. It contains the electronics for the actuation and presents a user-friendly interface to be easily used by an operator.

The electronics is controlled by an open-source prototyping platform, the Arduino Micro board (Arduino, Interaction Design Institute, Ivrea, Italy).

In the DALI system, the control box (Figure 18) allows (a) to regulate membrane cyclic stretching and (b) to read QCM parameters (frequency and temperature, see section 4.3.1.4).



Figure 18: Picture of the control box. The potentiometers allow to regulate the membrane stretching of two bioreactors in parallel. The stretching starts when pressing the stretching-button. The QCM-button allows the acquisition of QCM parameters (frequency and temperature), which are shown on the LCD.

a) Membrane actuation

Membrane displacement is possible thanks to an incoming airflow into the apical chamber (setup shown in Figure 19): an external source of controlled compressed air increases the pressure on the upper side of the membrane. In particular, the presence of commercial electropneumatic regulators (ITV0011-2BL, SMC, Italy) allows the control of the compressed air that flows into the apical chamber of the bioreactor through the inlet tube shown in Figure 7a. The outlet tube of the apical chamber is therefore closed by a clip (shown in Figure 7a) to avoid air outflow. In the control box, two electropneumatic regulators are placed for the stretching of two devices in parallel.

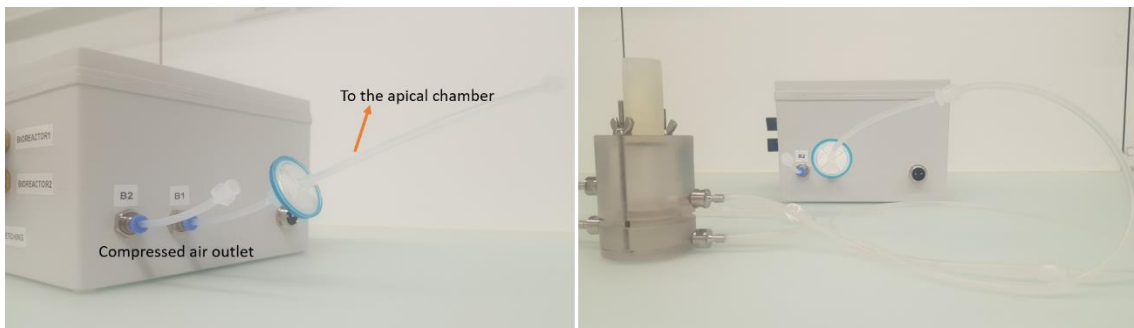


Figure 19: Bioreactor connected to the compressed air circuit. On the left is shown the compressed air outlets placed on the side of the control box. Picture on the right shows the connection between one of the outputs and the bioreactor.

The DALI system was designed to apply to the membrane different linear strains (<5%, 5-12%, 12-17% and >17%, Figure 20), allowing to mimic different conditions, both pathological and physiological. Setting the linear strain of the membrane lower than 5%, cells will be understretched, between 5-12% we are under physiologic conditions [1], while if we set the linear strain higher than 12% cells will be overstretched, reaching pathological conditions for stretching higher than 17% [1], [3].

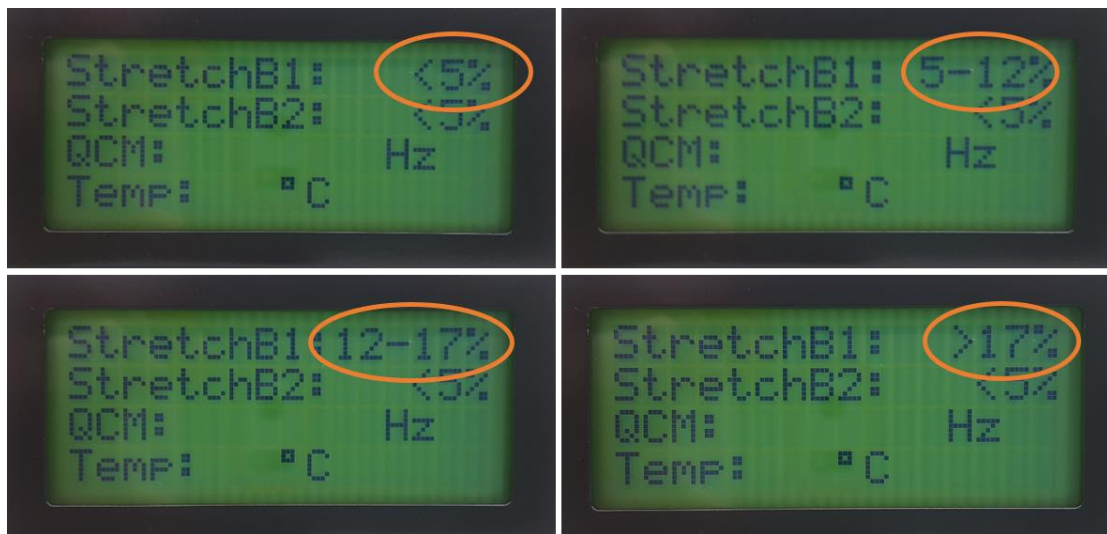


Figure 20: LCD on the control box showing the different linear strains that can be applied to the membrane.

Once selected the stretching entity and started the membrane actuation pressing the dedicated button, a cyclic deformation is applied to the membrane, mimicking the inhalation and exhalation phase (frequency = 0.2 Hz).

The commercial electropneumatic regulator used to control the inlet pressure in DALI system can regulate a constant inlet pressure (between 0.1 and 0.2 MPa) in a range from 0.001 to 0.1 MPa, through an analog electrical signal. As the maximum inlet pressure of the regulator is 0.2 MPa, a manometer is used to control the incoming air upstream of the control box (Figure 21).



Figure 21: A manometer is used to control the incoming air into the pressure regulators.

b) QCM parameters acquisition

As previously mentioned, it is possible to connect the QCM to the control box, without using the commercial controller QCM200 to analyse the frequency and resistance trends. In fact, the electronic placed inside the control box mounts a crystal oscillator driver (SN74LVC1GX04, Texas Instruments NanoStar™ and NanoFree™ Packages), which incorporates an unbuffered inverter plus an inverter into a single device and it is optimized for crystal oscillator applications in a wide range of frequency (e.g. 1-25 MHz). Furthermore, it is equipped with an I²C temperature sensor in order to better monitoring the temperature dependence of the quartz crystal frequency. The oscillator driver is optimized to work at 3.3 V supply voltage, ±24 mA output current. Both the oscillator driver and the temperature sensor are controlled by the microprocessor of Arduino Micro.

Finally, a user-friendly interface was designed to easily control the experimental setup and monitor device operations without the help of a computer (stand-alone system). It allows the setting of the membrane stretching entity and the acquisition of QCM parameters. In particular, the panel (Figure 18) is composed of:

- two potentiometers for controlling the stretching level of the membrane. There are two potentiometers as it is possible to regulate the membrane stretching of two bioreactors in parallel.
- Two LEDs, which indicate if the membrane is being stretched.

- Two buttons, one for the acquisition of the QCM parameters and one for starting the membrane stretching.
- An LCD display, where the experiment setup and the QCM parameters are shown.

Figure 22 shows the control diagram of the DALI system. As mentioned before, the control box can regulate the pressure within two bioreactors in parallel. Therefore, with labels *Stretching 1* and *2* in Figure 22 we refer to the stimuli applied to bioreactor 1 and 2, respectively. It is possible to set the stretching to be applied to the membrane using the potentiometers: when the stretching is started pressing the *Stretching button*, the LEDs turns on. LEDs 1 and 2 turn on when the bioreactor 1 and 2 are pressurised, respectively. The stretching is started and paused every 2.5s, to replicate the breathing frequency equal to 0.2 Hz for the entire breathing cycle (2.5s for the inhalation phase and 2.5s for the exhalation one).

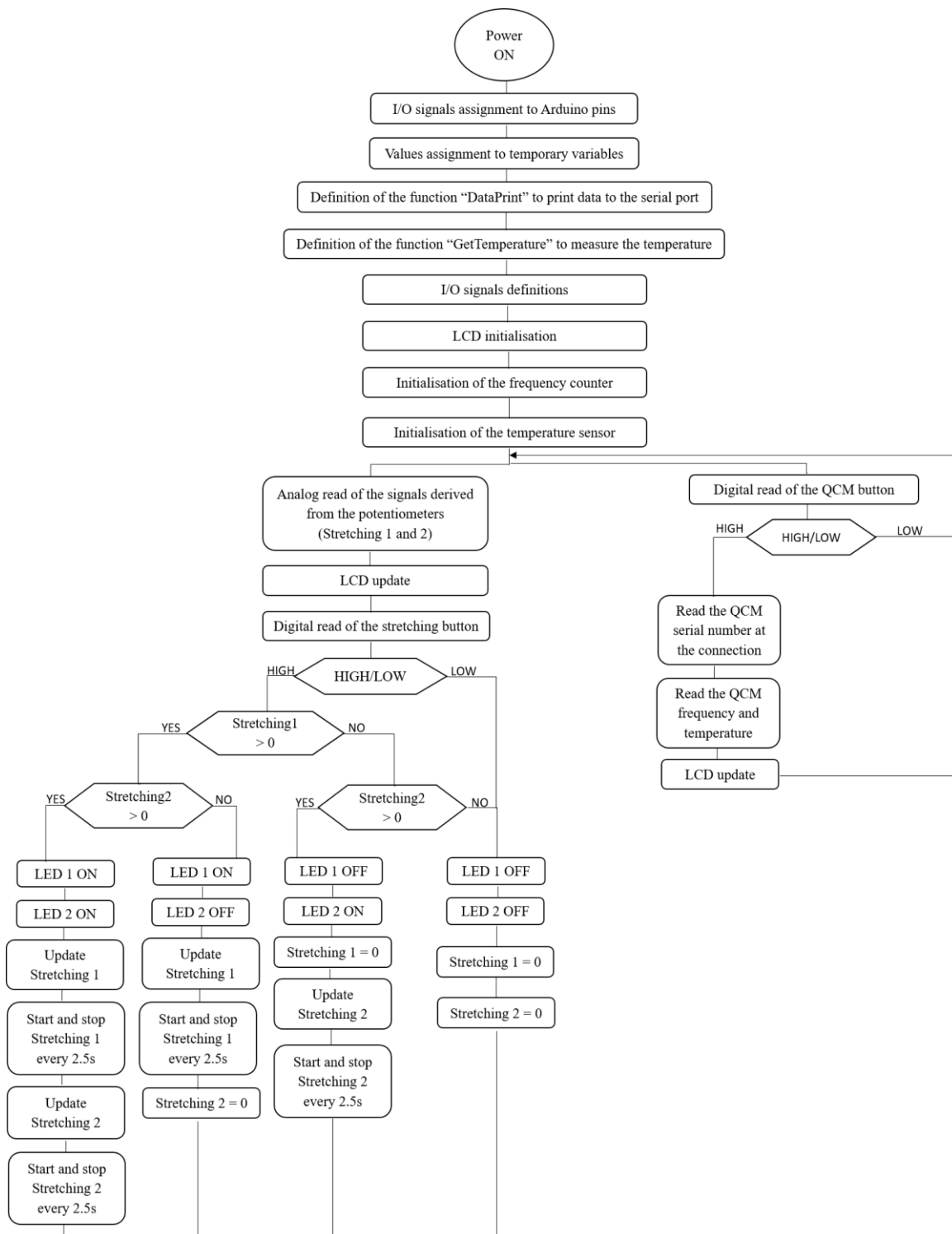


Figure 22: Control diagram of the DALI system. With Stretching 1 and 2 we refer to the stimuli applied to bioreactor 1 and 2, respectively.

4.3.2 Calibration of the membrane stretching system

After fabricating the bioreactor, it was essential to calibrate its actuation system, in order to know the pressure to apply to the apical chamber for having the desired

buckling of the membrane. Therefore, the electropneumatic regulator was calibrated, correlating the digital actuation with the pressure inside the upper chamber, and consequently the membrane displacement. An infrared laser (GP2Y0A51SK0F, Sharp Electronics S.p.A., Milan, Italy, Figure 23) was used to measure the membrane displacement according to the pressure applied. GP2Y0A51SK0F is a distance measuring sensor unit, composed of an integrated combination of PSD (Position Sensitive Detector), IR-LED (Infrared Emitting Diode) and signal processing circuit. This device outputs the voltage corresponding to the detection distance. Table 4 shows the electro-optical characteristics of the sensor. As the maximum output voltage of the sensor is low ($V_{\max} = 1.95V + 0.55V = 2.5V$, see Table 4), during sensor calibration it was amplified using an operational amplifier (OP07) with gain 2 ($V_{\text{final}} = 5V$).

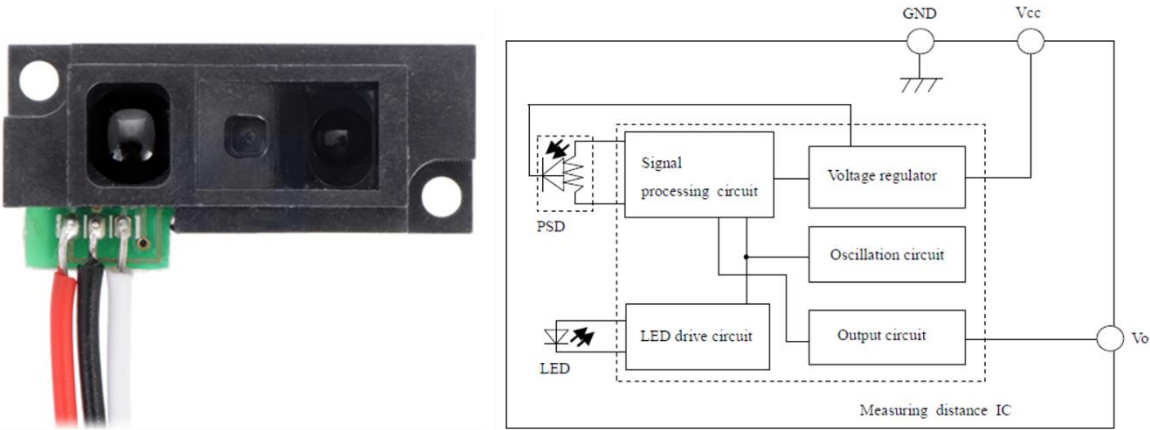


Figure 23: GP2Y0A51SK0F infrared sensor and its schematic.

Table 4: Electro-optical characteristics of the sensor.

Parameter	Symbol	Conditions	Min.	Typ.	Max.	Unit
Measuring distance range	ΔL	-	2	-	15	cm
Output terminal voltage	V_0	$L=15\text{ cm}$	0.25	0.4	0.55	V
Output voltage difference	ΔV_0	$15 \rightarrow 2\text{ cm}$	1.35	1.65	1.95	V

A manual linear micropositioner (Figure 24A) was used to calibrate the sensor, whose voltage output was read by a sketch implemented with Arduino. The sensor was fixed on the top of the bioreactor upper chamber, in correspondence of the hole

that houses the nebulizer. This hole was closed with a transparent polycarbonate cap, upon which the sensor was attached (Figure 24 B and C). The cap was transparent to ensure the transmission of infrared rays. Finally, a white sheet fixed in the membrane holder was used as reference and attached to the moving component of the positioner (Figure 24 B and C).

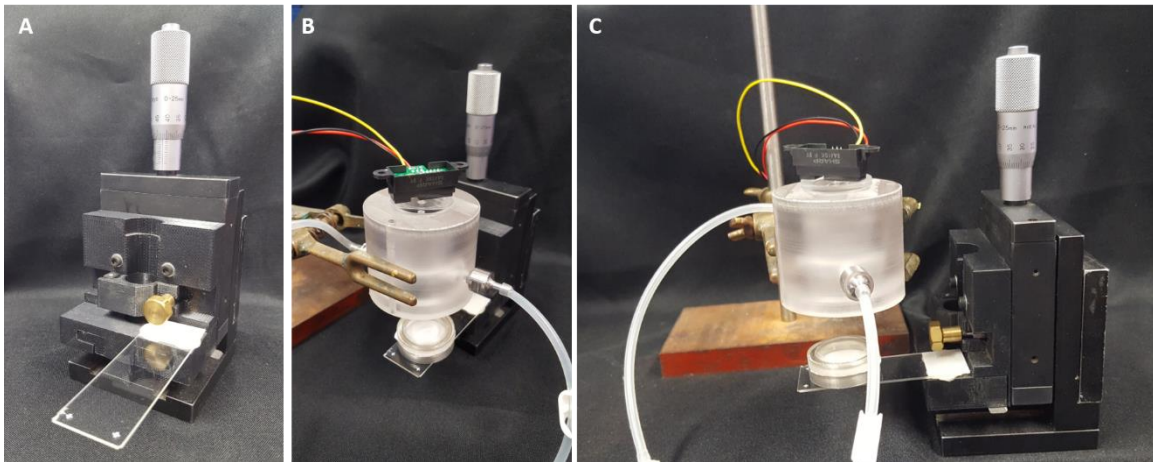


Figure 24: A) picture of the micropositioner used to calibrate the infrared sensor. B) and C) setup used to calibrate the infrared sensor: the sensor attached to the upper chamber is kept in a fixed position, while the reference (white sheet fixed in the holder) is moved with the positioner.

The distance between the sensor and the reference was increased by a fixed step of 1 mm using the micropositioner. In this way, it was possible to correlate a known distance with the output voltage of the sensor, thus the bits read by Arduino. The solid line in Figure 25 shows the correlation displacement-bit, while the dotted line represents its linear approximation (calibration line). The obtained calibration line was used to calculate the detection distance as follow (Eq. 10):

$$D_{mm} = \frac{D_{bit} - 507.77}{-6.68} \quad (10)$$

Where D_{bit} is the analog signal read by Arduino, which is proportional to the distance (D_{mm}) between the sensor and the reference.

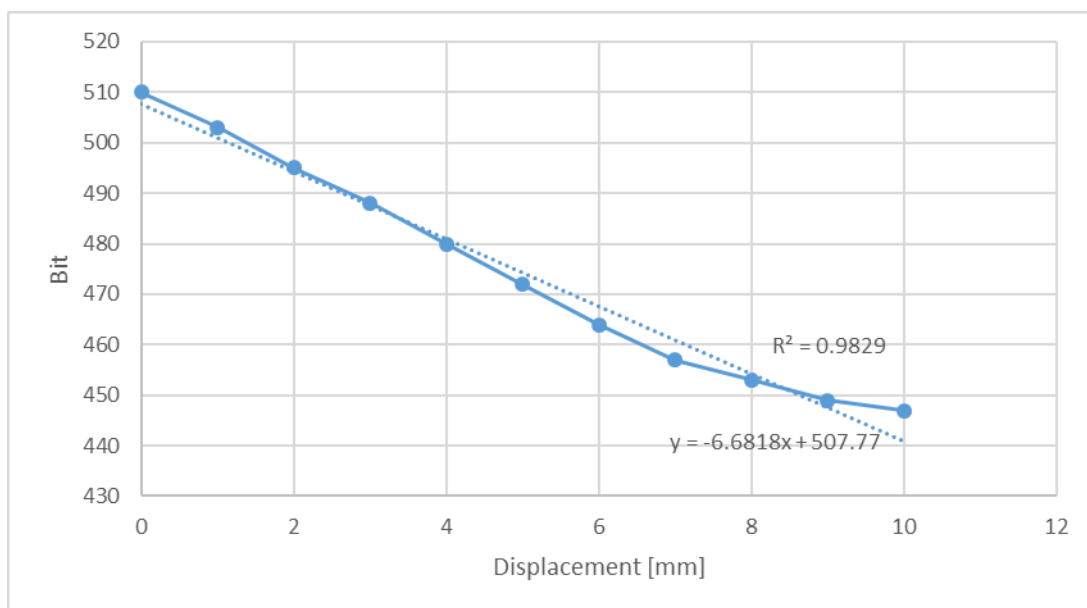


Figure 25: Calibration line of the GP2Y0A51SK0F infrared sensor. The solid line represents the correlation bit-displacement, while the dotted line its linear approximation (calibration line). The equation of the calibration line is shown, as well as the coefficient of determination R^2 .

Once obtained the calibration line, the sensor was used to correlate the membrane displacement to the pressure applied to the apical chamber. To do so, the sensor was fixed on the top of the bioreactor, as shown in Figure 26.



Figure 26: Setup used to correlate the membrane displacement to the pressure applied to the apical chamber.

The previously determined calibration line was used to measure the displacement of the membrane due to the pressure increase. However, as the zero position of the sensor placed on the bioreactor was different with respect the setup used during the previously calibration, the new zero point was found reading the analog signal of the

sensor before starting the pressurisation. The new calibration line is the following (Eq. 11), where the slope of the line is the same as before:

$$D_{mm} = \frac{D_{bit} - 517.85}{-6.68} \quad (11)$$

Then, an Arduino sketch was used to increase the input voltage of the pressure sensor ($V_{in} = 0.5 \text{ V}$, $V_{fin} = 5 \text{ V}$, $\text{step} = 0.5 \text{ V}$), therefore its output pressure, leading to the membrane displacement. Reading the analog output of the infrared sensor allowed to correlate the input voltage of the pressure regulator with the membrane displacement, finding the following correlation line (Eq. 12):

$$D_{mm} = 3.99 V_{applied} \quad (12)$$

Using this equation, it is possible to know the input voltage to apply to the pressure regulator in order to have the desired axial displacement of the membrane (see section 4.3.1).

4.3.3 QCM characterization and validation

After designing and fabricating the Quartz Crystal Microbalance, the device was characterized and validated to verify its suitability to quantify the amount of nanoparticles aerosolized on the cell layer. Therefore, the lower limit of the linearity range of the QCM was measured, in order to verify it was small enough to ensure the linearity of the measurements considering our aerosolized quantities. Moreover, the blank of the device was calculated, since it will be subtracted during exposure experiments. Finally, preliminary experiments were performed, during which nanoparticles have been aerosolized to verify the device suitability in terms of mass detection.

4.3.3.1 Calculation of the lower limit of the linearity range of the QCM

The lower limit of the linearity range of the QCM was measured, in order to verify the feasibility of working in a linear range when aerosolizing small amount of particles.

First, the QCM was assembled as shown in section 4.3.1.3 and connected to the QCM200 controller. Since the aerosolization on the cell layer is performed at 37°C , the QCM was positioned on a hot plate ($T=37^{\circ}\text{C}$) to reproduce experimental nebulisation conditions (setup shown in Figure 27). The software was turned on,

starting the reading of frequencies values. An hour has been waited before nebulizing any substance to allow device stabilization.

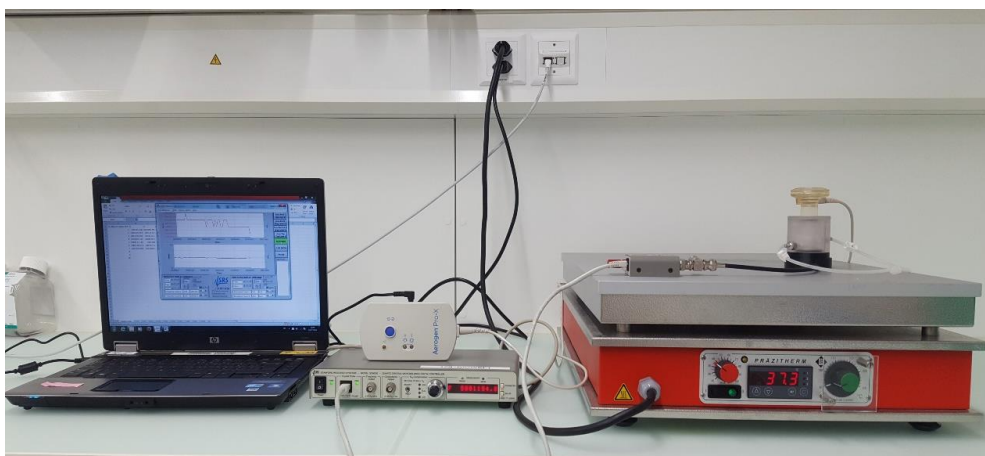


Figure 27: Experimental setup during tests with the QCM.

According to the Sauerbrey equation (see section 4.3.1.3), the deposited mass is correlated to the changes in the oscillation frequency of the piezoelectric crystal. Therefore, to determine the mass deposited, the frequency has been acquired before and after particle deposition (Δf). A solution of 0.9% NaCl (w/V in distilled water) was diluted in distilled water (dH₂O): 0.3, 0.4, 0.5, 1, 2, 3, 4, 5 and 6 μL of 0.9% NaCl were dissolved in 100 μL of dH₂O. Then, 10 μL of each solution was pipetted in the Aeroneb Pro and nebulized on the membrane. The solution was completely nebulized in 5 seconds. Table 5 reports frequency and mass values correlated to each different concentration of the nebulized solutions, while Figure 28 shows the trend of the mass respect to the solution concentration.

Table 5: Frequency and mass values correlated to each different concentration of the nebulized solutions. In bold the lower limit of the linearity range.

0.9% NaCl concentration [$\mu\text{L}/100\mu\text{L}$ dH ₂ O]	Δf [Hz]	m [$\mu\text{g}/\text{cm}^2$]
0.3	2.1151	0.0374
0.4	1.6413	0.0290
0.5	5.0989	0.0900
1	9.4625	0.1672
2	16.9348	0.2992
3	20.5370	0.3628
4	29.5411	0.5219
5	31.3665	0.5542
6	41.0952	0.7261

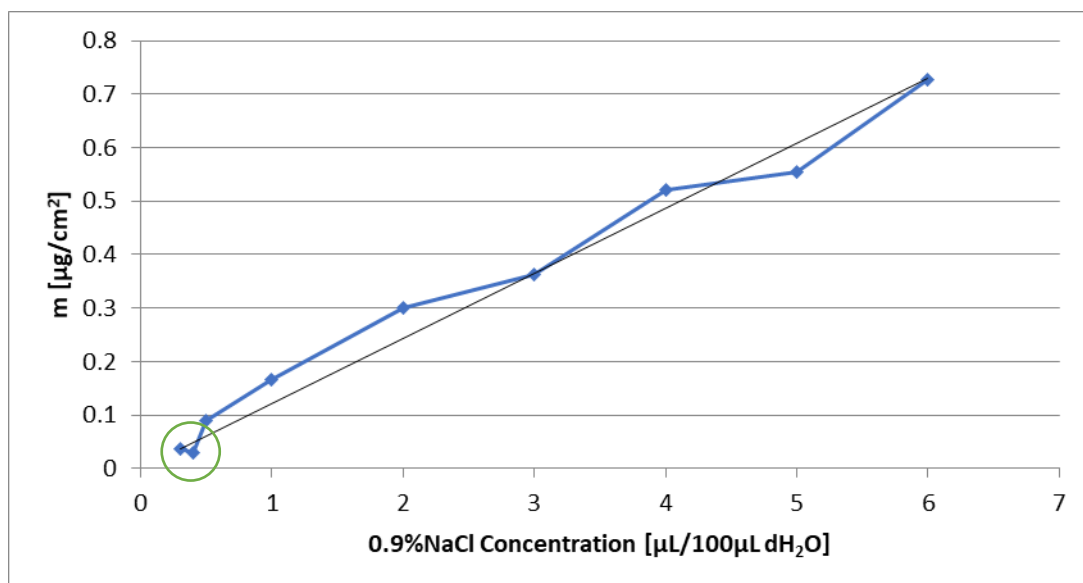


Figure 28: Trend of the mass respect to the solution concentration. In the circle, the concentration at which the mass trend is no more linear.

Evaluating mass trend in Figure 28, it is possible to conclude that, when the amount of 0.9% NaCl diluted in dH₂O and then nebulized was lower than 0.4 $\mu\text{L}/100\mu\text{L}$ (values in the orange circle in Figure 28), the mass trend was no longer linear, indicating that value as the lower limit of the linearity range. It corresponds to a mass equal to 0.029 $\mu\text{g}/\text{cm}^2$, as showed in bold in Table 5.

4.3.3.2 Blank detection of the QCM

When nebulizing nanoparticles, they are usually dissolved in a batch solution of 1% of 0.9%NaCl (w/V in dH₂O) dissolved or in dH₂O or in 0.05% BSA (Bovine Serum Albumin, w/V in dH₂O). Therefore, it is necessary to subtract the blank to know the exact mass of deposited nanoparticles. First, the blank derived from the solution of 0.9% NaCl diluted in dH₂O was determined. Using the QCM experimental setup shown in Figure 27, 1 μL of 0.9% NaCl was dissolved in 100 μL of dH₂O. Then, 10 μL of this solution were pipetted in the Aerogen Pro and nebulized on the quartz crystal. To calculate the mass, frequencies values were acquired before and after the nebulisation. This procedure was repeated for 10 times, in order to obtain the average blank mass. The same steps were followed to detect the blank when dissolving 0.9% NaCl in 0.05% BSA. Tables 6 and 7 show the masses obtained nebulizing 10 μL of solutions of NaCl dissolved in dH₂O and 0.05% BSA respectively.

Table 6: Frequency and mass values obtained nebulizing a solution of 1% of 0.9% NaCl dissolved in dH₂O.

# Repetition	Δf [Hz]	m [$\mu\text{g}/\text{cm}^2$]
1	12.9290	0.2284
2	12.9731	0.2292
3	13.3296	0.2355
4	9.4625	0.1672
5	11.5252	0.2036
6	7.2581	0.1282
7	11.2061	0.1980
8	9.9318	0.1755
9	10.0253	0.1771
10	7.2375	0.1279

Table 7: Frequency and mass values obtained nebulizing a solution of 1% of 0.9% NaCl dissolved in 0.05% BSA.

# Repetition	Δf [Hz]	m [$\mu\text{g}/\text{cm}^2$]
1	24.4813	0.4325
2	24.1331	0.4264
3	33.1008	0.5848
4	28.8785	0.5102
5	33.1754	0.5861
6	29.4469	0.5203
7	40.1978	0.7102
8	30.6413	0.5414
9	32.9494	0.5821
10	32.4121	0.5727

Averaging mass values shown in Tables 6 and 7, the blank derived from the solution in dH₂O is equal to $0.1870 \pm 0.0391 \mu\text{g}/\text{cm}^2$, while the blank of the solution in 0.05% BSA is equal to $0.5467 \pm 0.0825 \mu\text{g}/\text{cm}^2$. The standard deviation is low in both the cases, suggesting the reproducibility of the measurements obtained with the designed device.

4.3.3.3 Measuring nanoparticle deposition using the designed QCM

Once determined the lower limit of the linearity range of the device and the blank to subtract, tests measuring nanoparticles deposition were performed to validate the designed QCM, using the setup shown in Figure 27. Barium sulphate (BaSO₄) was

selected as particle to be aerosolized. Three solutions with different BaSO₄ concentrations were tested: 0.5, 1 and 2.56 mg/mL of BaSO₄ dissolved in dH₂O. In detail, 100 µL of each solution were mixed with 1 µL of 0.9% NaCl; then 10 µL of these solutions were pipetted in the Aerogen Pro and nebulized on the crystal. Each mass measurement related to a specific concentration was repeated for 3 times. The measured masses are reported in Table 8 (the blank has already been subtracted from the values reported), while Figure 29 shows mass trend with respect to the BaSO₄ concentration.

Table 8: Measured masses after nebulisation of solutions with different BaSO₄ concentrations.

BaSO ₄ concentration [mg/mL dH ₂ O]	m [µg/cm ²]
0.5	0.0240±0.0203
1	0.4625±0.0841
2.56	0.8956±0.1250

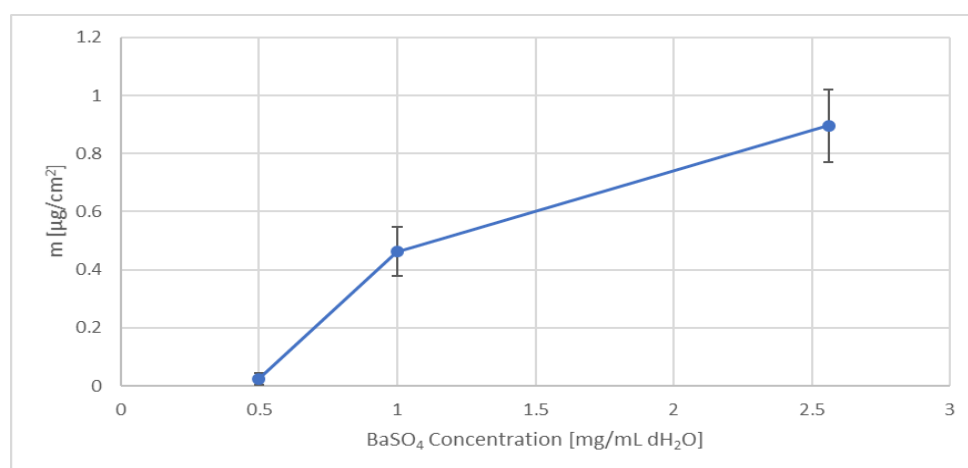


Figure 29: Mass trend with respect to the BaSO₄ concentration.

The results show a low standard deviation, with an increasing measured mass with the increase of barium sulphate concentration, as expected. This suggests that the device is suitable to quantify the amount of aerosolized particles in an accurate fashion.

4.3.4 Liquid and air tightness of the bioreactor

Liquid and air tightness were tested to guarantee the correct flow and pressure inside the chambers and to avoid cell contamination due to a contact with chemical or biological contaminants.

The water tightness was evaluated connecting the bioreactor to a peristaltic pump (Ismatec IPC 4, IDEX Health & Science, Germany), and testing the fluidic system at different flow velocities. A PBS solution was circulated at a flow rate in a range between 100 and 400 $\mu\text{L}/\text{min}$ (which is the maximum flow range applied during dynamic cell culture [4]), with an increasing step of 100 $\mu\text{L}/\text{min}$. The complete system was left on for 24 hours, and the absence of water droplets outside the bioreactor was checked with blotting paper. The bioreactor turned out to be watertight for the entire considered flow range and duration of the experiment.

Airtightness was ensured by connecting the apical chamber to the control box, thus to the compressed air circuit. The stretching level was set at the maximum applicable (>17%), and the bioreactor was immersed in a container filled of water. When the stretching was started and the air entered inside the bioreactor, no air bubbles were observed in the water, meaning there was no air leakage.

5 References

- [1] E. Roan and C. M. Waters, "What do we know about mechanical strain in lung alveoli?," *Am. J. Physiol. Lung Cell. Mol. Physiol.*, vol. 301, no. 5, pp. L625-35, 2011, doi: 10.1152/ajplung.00105.2011.
- [2] K. G. Birukov *et al.*, "Magnitude-dependent regulation of pulmonary endothelial cell barrier function by cyclic stretch," *Am. J. Physiol. - Lung Cell. Mol. Physiol.*, 2003.
- [3] M. Felder *et al.*, "Impaired wound healing of alveolar lung epithelial cells in a breathing lung-on-a-chip," *Front. Bioeng. Biotechnol.*, vol. 7, no. JAN, pp. 1–5, 2019, doi: 10.3389/fbioe.2019.00003.
- [4] D. Mazzei, M. A. Guzzardi, S. Giusti, and A. Ahluwalia, "A low shear stress modular bioreactor for connected cell culture under high flow rates," *Biotechnol. Bioeng.*, vol. 106, no. 1, pp. 127–137, 2010, doi: 10.1002/bit.22671.
- [5] P. F. Davies and S. C. Tripathi, "Mechanical stress mechanisms and the cell: An endothelial paradigm," *Circulation Research*. 1993, doi: 10.1161/01.res.72.2.239.
- [6] D. D. Nalayanda, C. M. Puleo, W. B. Fulton, T. H. Wang, and F. Abdullah, "Characterization of pulmonary cell growth parameters in a continuous perfusion microfluidic environment," *Exp. Lung Res.*, 2007, doi: 10.1080/01902140701557754.